Corrosion Science 184 (2021) 109390

Contents lists available at ScienceDirect

Corrosion Science

journal homepage: www.elsevier.com/locate/corsci

Corrosion-induced microstructure degradation of copper in sulfide-containing simulated anoxic groundwater studied by synchrotron high-energy X-ray diffraction and *ab-initio* density functional theory calculation

Fan Zhang [a], Cem Örnek [b], Min Liu [a], Timo Müller [c], Ulrich Lienert [c], Vilma Ratia-Hanby [d], Leena Carpén [d], Elisa Isotahdon [d], Jinshan Pan [a,*]

[a] KTH Royal Institute of Technology, Division of Surface and Corrosion Science, Stockholm, Sweden
[b] Istanbul Technical University, Department of Metallurgical and Materials Engineering, Istanbul, Turkey
[c] Deutsches Elektronen-Synchrotron (DESY), Photon Science, Hamburg, Germany
[d] VTT Technical Research Centre of Finland, Espoo, Finland

ARTICLE INFO

Keywords:
Copper canister
Hydrogen infusion
Lattice degradation
Nuclear waste
HEXRD
DFT

ABSTRACT

Synchrotron high-energy XRD measurements and ab-initio DFT calculations were employed to investigate microstructural degradation of copper upon exposure to sulfide-containing anoxic groundwater simulating nuclear waste repository. After two-month exposure, the high-energy XRD measurements revealed heterogeneous lattice deformation in the microstructure and lattice expansion in near-surface regions. The DFT calculations show that sulfur promotes hydrogen adsorption on copper. Water causes surface reconstruction and promotes hydrogen insertion into the microstructure, occurring via interstitial sites next to vacancies leading to lattice dilation and metal bond weakening. Hydrogen infusion in the presence of sulfur caused lattice degradation, indicating a risk for H-induced cracking.

1. Introduction

A large amount of spent fuel is produced every year from commercial nuclear power plants, 1% of the nuclear waste is highly radioactive and its safe disposal is as important as nuclear safety. Deep geological disposal is the prefered approach for permanent storage of the nuclear waste in several countries. Governmental regulations stipulate safe long-term isolation of nuclear waste for a minimum of 100,000 years, which imposes a great engineering challenge. The nuclear waste disposal concept in Sweden and Finland is based on a multi-barrier system, where the spent fuel is first placed in cast-iron inserts, which are then inserted into canisters as a barrier to seal the cast-iron inserts. The canisters will be placed in bedrock in the depth of 400–1000 meters, surrounded by bentonite clay buffer, to achieve the isolation from the human living environment [1–3]. High-purity copper has been chosen for fabricating the canisters that will be placed under granite environments at anaerobic reduction and anoxic aqueous conditions [4]. The compacted bentonite clay acts as a sealing material providing another barrier separating groundwater and the canisters, buffering minor movements of the repository system, and retaining eventual release of nuclides upon canister failure [2,3]. The bedrock is considered stable and durable, providing an outer barrier of the multi-barrier structure between nuclear waste and the biosphere.

For the safety assessment, corrosion of copper under oxic and anoxic conditions, and radiation-influenced and microbiologically-influenced corrosion have been intensively investigated over 40 years [5–11]. A recent review gives an overview of the corrosion issues, debated questions, and ongoing research programs [12]. A number of reports assessing corrosion of copper canister under expected repository conditions with conservative assumptions, often using a uniform corrosion rate in the calculation of corrosion allowance, have concluded that there is no considerable risk for canister failure [12]. However, the risks for several complex forms of copper corrosion have been debated in the Land and Environmental Court of Sweden, leading to the statement to the Swedish Government, that supplementary information related to the long-term behaviour of the copper canisters should be presented and

* Corresponding author.
E-mail address: jinshanp@kth.se (J. Pan).

https://doi.org/10.1016/j.corsci.2021.109390
Received 29 November 2020; Received in revised form 2 March 2021; Accepted 10 March 2021
Available online 15 March 2021

evaluated regarding five issues: i) corrosion due to reaction in oxygen-free water; ii) pitting due to reaction with sulphide; iii) stress corrosion cracking due to reaction with sulphide; iv) hydrogen embrittlement; v) the effect of radioactive radiation on pitting, stress corrosion cracking and hydrogen embrittlement [13]. Clearly, there is a need to gain a deep understanding of the role of sulphur and hydrogen in stress corrosion cracking (SCC) and hydrogen embrittlement of copper in the ground water containing sulphide.

To cover all aspects of safety assessment, it is necessary to evaluate the scenarios when cracks are present in the rock and the bentonite is swelling with groundwater, so copper canisters get into contact with groundwater and even microbes where bentonite sealing could be damaged. Microbial activity on the surface or in the vicinity of the canister was modeled [14], and it was reported to initiate and accelerate general and localized corrosion [15]. Oxygen exists in the initial period of the repository closure and is gradually consumed by oxidation reactions and microorganisms [12]. Oxidation of copper can result in a surface film of Cu_2O or $CuO/Cu(OH)_2$. Once the trapped oxygen is completely consumed, the major threat to the long-term durability of the canister is corrosion by sulfide species (e.g., HS^-) produced in the groundwater by mineral dissolution and/or microbial activity of, e.g., sulfate-reducing bacteria and methanogens in the repository environment [12,16]. Sulfide is known to be a corrosive agent causing SCC of copper in anaerobic chloride containing environments [8,9,17]. Previous studies have shown the role of sulfate-reducing microorganisms [18,19], and biotically-induced formation of Cu_2S layer [20,21], in the corrosion of copper. The sulfide leads to corrosion of copper, forming stable and insoluble sulfides [22–24], e.g.,

$$2Cu + S^{2-} \rightarrow Cu_2S + 2e^- \quad (1)$$

The sulphide-induced corrosion process can be sustained by cathodic reduction of water or HS^-.

$$2H_2O + 2e^- \rightarrow H_2 + 2OH^- \quad (2)$$

$$2HS^- + 2e^- \rightarrow H_2 + 2S^{2-} \quad (3)$$

Studies on copper corrosion often focused on chemical and electrochemical degradation at the copper/electrolyte interface [25,26]. It was also reported that sulfide-induced corrosion might also have a significant influence on the bulk material of copper. Chemical conversion of a film of Cu_2O to Cu_2S on copper has been shown to proceed to completion and extend deep into the bulk Cu [27]. The conversion was observed to extend into the sub-surface region as deep as 100 nm [28]. Moreover, hydrogen may be produced when copper corrodes in the presence of sulfide. In general, hydrogen has detrimental effects on mechanical properties of copper and can create bubbles and microcracks of copper materials [29–32]. Adsorption and diffusion of hydrogen in copper depend on the surface condition and microstructural defects such as dislocations and inclusions, and grain boundaries are primary trapping sites of hydrogen [33,34]. Hydrogen-induced damage of copper canister has, so far, been considered to be negligible due to the belief that the permeation depth of hydrogen would be too small to influence the mechanical integrity of copper canister [35,36]. However, the previously used method only yielded depth-profiles of hydrogen [33,36], but no information about its role in the SCC and hydrogen embrittlement of copper. In the presence of tensile stress/strain, exposure to ground water containing sulfide can cause SCC of copper [8,9,17]. To achieve an atomistic understanding of the mechanism of the SCC and hydrogen embrittlement, it is necessary to study corrosion-induced lattice degradation of copper, particularly the role of sulfur and hydrogen. To our knowledge, this has not been done before.

Here, we report synchrotron high-energy X-ray diffraction (HEXRD) measurements in transmission mode and *ab-initio* density functional theory (DFT) calculations to investigate the effect of exposure to simulated anoxic groundwater containing sulfide on the lattice degradation of copper. The interatomic lattice distances (d-spacing) were measured in 20 μm increments through the entire two-mm thick sample to reveal an in-depth gradient of the lattice deformation and thus the extent of the exposure-induced lattice degradation. DFT calculations of Cu-S-H systems (also in water) were carried out to provide an atomistic understanding of the surface adsorption, dissociation, and infusion of hydrogen that lead to degradation of the Cu lattice.

2. Experimental

2.1. Material used

The tested material was hot rolled, oxygen-free, phosphorus-containing copper (> 99.95 wt.% Cu, 0.005 wt.% P), which is the material used for making canisters, and provided by Finnish nuclear waste management company Posiva Oy. The specimens were cut into approximately 10 mm × 10 mm × 2 mm, and the surface was ground and polished down to 1 μm finishing. Prior to exposure, the specimens were cleaned in acetone and ethanol. The copper material had a typical hot-rolled microstructure, with large grains (several tens to hundreds of micrometers in size) and annealing twins, as seen in Fig. 1. As-polished and pre-oxidized samples were investigated. The pre-oxidation was done at 90 °C in ambient air for seven days after the polishing to simulate the effect of exposure to oxic conditions prior to the anoxic stage. It was previously observed that the pre-oxidation increased mass loss of copper specimens during exposure to anoxic conditions [37].

2.2. Corrosion exposure

The specimens were exposed to simulated groundwater in a sealed bottle for 53 days. The chemical components of the water are given in Table 1, which represent the groundwater of the Finnish disposal site and the effects of added bentonite. Sulfide was added in the form of Na_2S with a concentration of 10^{-3} mol/L (32 mg/L). The exposure was done at room temperature (22 °C) in a laboratory-grade borosilicate glass bottle with a volume of 2 L. The experiment environment was anoxic, achieved by purging the water and the vessel with argon before the start of the test and sealing the vessel with butyl rubber stopper.

2.3. High-energy X-ray diffraction experiment

HEXRD measurements were carried out at the Swedish Materials Science beamline P21.2 at PETRA III of the DESY, Hamburg, Germany. The photon energy was 96 keV (corresponding to 0.1291 Å). The distance between the sample and the Varex 4343CT flat panel detector was about 1.6 m. LaB6 was used for geometrical calibration. The sample surface was aligned to be parallel to the X-ray beam. The sample was

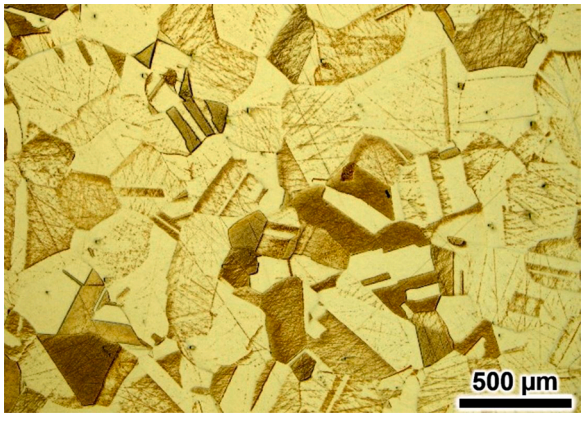

Fig. 1. Optical micrograph of an etched copper sample showing typical microstructure (large grains and annealing twins) of canister material.

Table 1
Chemical components of the used simulated groundwater.

	K	Ca	Cl	Na	SO_4	Br	HCO_3	Mg	Sr	Si	B	F	Mn	PO_4	S	lactate
mg/L	54.7	280.0	5274.0	3226.1	595.0	42.3	13.7	100.0	8.8	3.1	1.1	0.8	0.2	0.1	32.0	1.0

positioned 45° towards the beam with respect to its vertical rotational axis and illuminated 1.5 mm away from the edge to reduce the effective sample depth for transmission to about 3 mm. The beam size was 20 μm (vertical) x 55 μm (horizontal). The sample surface was defined as the position where the intensity of the transmitted beam through the specimen had its half intensity when sampling across the sample surface. The sample was moved vertically in steps of 20 μm (z-axis). At each z-position (height), a 2-D diffraction pattern was recorded with a sampling time of 1 s. During each data sampling, the sample was moved by 1 mm along the horizontal axis (parallel to the surface) to improve grain statistics, resulting overall in a serpentine sample movement (transmission was kept less than 3 mm). The measurement at the surface yields diffraction signals from approximately 10 μm beneath the surface and all other measurement points include signals from a volume of 20 μm height. The measurement time for each scanned layer was 3.8–4.0 s, including the summation of sampling time and dead time for stage movement. The sample was scanned from 150 μm above the upper-side surface down to 150 μm below the lower-side surface to capture the entire specimen. The measurement setup is schematically illustrated in Fig. 2. The diffraction patterns were collected and stored as tiff files, which were then integrated azimuthally in a range of ±5° using pyFAI [38]. The diffraction data were also integrated over the entire azimuth full-circle (0–360°). The intensities were normalized using the primary beam intensity, which was collected simultaneously to compensate beam fluctuation. All images were background subtracted. Data analysis was performed using the Peak Analyzer module Fit Peaks (Pro) of OriginPro 2020b V9.7.5.184 software, utilizing a mixture algorithm of Lorentzian and Gaussian peaks for fitting, which gave the best fitting quality. The *d*-spacing was determined from the position of the 111 Bragg peak. The full-ring integration provided average but statistically relevant information about the changes in the lattice size. The d-spacings of the non-exposed specimen was taken as the reference point, and all the relative changes of the lattice parameter were calculated with respect to the non-exposed condition.

3. DFT calculation

DFT calculation was performed to study the surface adsorption and dissociation of S-components (H_2S and HS) on Cu(110) surface and the infusion of H into the Cu lattice, to achieve an atomistic understanding of the effect of S and H on the lattice degradation. Cu(110) surface was chosen in the calculation for easy comparison with literature reports, and the results differ only slightly for other surface orientations. Two types of interactions of H_2S with Cu were considered, i.e., the adsorption at the Cu(110) surface, and the insertion into defects in the Cu subsurface region. The Cu surface was modelled by a six-layer slab orientated at 110, which contains 36 Cu atoms, which is commonly used in DFT calculations of Cu. A vacuum layer equal to about two times the height of the slab was added to the calculation model. The Dmol3 code was used to theoretically investigate the interaction between environments and Cu [39,40], where the generalized gradient approximation (GGA) with PW91 exchange-correlation function [41] was applied, and a k-point of 3 × 6 × 1 was selected in the calculation. All the core electrons in the system were treated with DFT semi-core pseudopotentials. Optimization was regarded to be complete when the energy, residual force and displacement of each atom of the system converged to 10^{-5} Hartree (Ha), 0.002 Ha/Å, and 0.005 Å, respectively.

4. Results and discussion

4.1. Deformation of Cu lattice

From the HEXRD data, d-spacing of the Cu lattice was determined. Fig. 3 displays polar *d*-spacing plots of a non-exposed sample (reference), a pre-oxidized sample (oxidized), and a pre-oxidized sample after the exposure to the simulated groundwater (exposed or sulfur-exposed). The polar plots show the calculated d-spacing as a function of the azimuthal angle and depth from the surface of the sample. The vertical axis on the left of each polar plot (depth information) indicates the position inside the sample, with units in microns. The depth axis is radial, with 0 μm showing the sample surface. The increasing number of depths indicates the measured d-spacing below the surface. The polar plot shows the measured d-spacing for down to 1000 μm in bulk. The azimuth angle is plotted in the hoop-direction. The color code represents the magnitude of d-spacing, with the lattice size increasing from cold to hot colors. The outer ring of the polar plot shows the d-spacings for the surface along with all azimuth angles.

The non-exposed reference sample (Fig. 3a) shows quite uniform *d*-

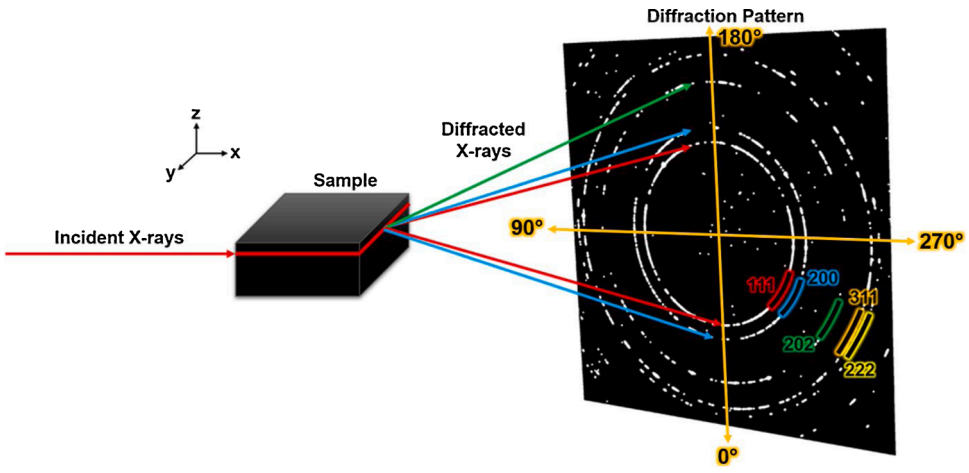

Fig. 2. Schematic illustration of the experimental setup for the HEXRD measurements showing X-rays radiating the copper specimen and the diffracted X-rays with the 2D diffraction pattern collected by a flat-panel detector. The azimuth angles are indicated.

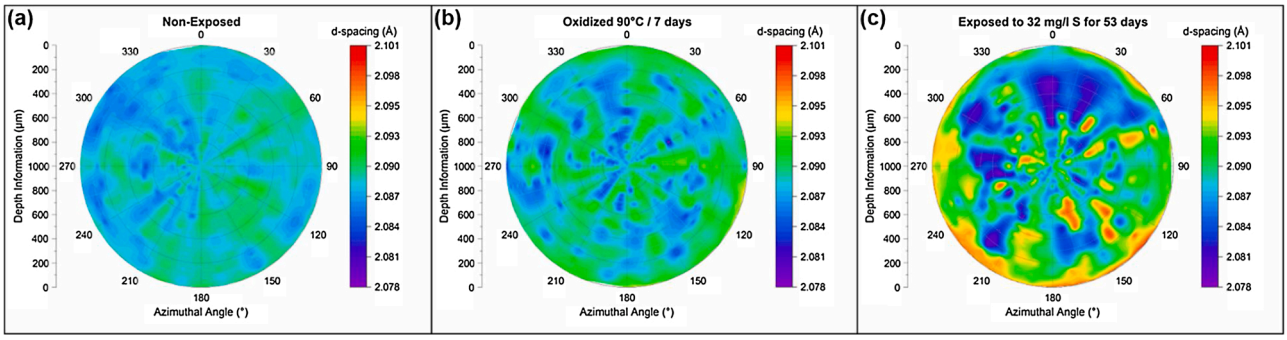

Fig. 3. Polar plots showing the calculated d-spacing of the Bragg peak with (111) orientation as a function of depth from the surface and azimuthal angle for the copper specimens of (a) the non-exposed condition, (b) pre-oxidized at 90 °C for seven days, and (c) pre-oxidized and exposed to 32 mg/l of sulfide-containing groundwater.

spacing values expected for the Cu lattice, with small deviations across the measured depth reflecting the heterogeneities in the microstructure, such as grain boundaries and grains in different sizes as shown in Fig. 1. In contrast, the magnitude and scatter of the *d*-spacings increased for the pre-oxidized sample (Fig. 3b). The sulfur-exposed sample had the largest *d*-spacings, indicating most degradation (Fig. 3c). While the pre-oxidation affected the near-surface region down to a depth of 20−40 µm (see also Fig. 5), the sulfur-exposure resulted in large lattice expansion down to 400 µm, with some expansion occurred on individual sites in the microstructure between 400 µm and 900 µm in depth. It seems that compensating lattice contraction occurred in the sub-surface microstructure as compared to the non-exposed and pre-oxidized specimens (Fig. 3c). Hence, the exposure to the simulated groundwater caused both heterogeneous lattice expansion and contraction. The size of the large grains of the microstructure was 200−500 µm and thus much larger than the X-ray beam size (20 µm × 55 µm), which explains the discrete heterogeneities in the d-spacings. Each scan line contained signals form approximately 50–100 grains, which is well-representative for the entire microstructure. Compensating lattice contraction, to a small extent, was also observed for the pre-oxidized specimen (Fig. 3b).

The lattice expansion, measured in the exposed specimen, showed a preferential azimuthal orientation. The lattice expansion was more pronounced along with the azimuthal angles 120−240°, which means that the lattice expanded orthogonal to the exposed surface. The increase of the interatomic distance of the lattice implies grain elongation due to directional strain formation, which is likely induced by the infusion of H, and possibly also S and/or O atoms, from the environment into the lattice of the Cu (discussed in the sections below).

Furthermore, the change of the *d*-spacing was used to calculate the relative change of the lattice parameter at different depths, which includes strain development due to H insertion into the lattice. As shown in Fig. 4, the pre-oxidation caused lattice expansion of the surface region, evidenced by positive values of the relative lattice change at most azimuthal angles (Fig. 4a). In contrast, the sulfur-exposure resulted in both lattice expansion and contraction in the surface region (Fig. 4a) and

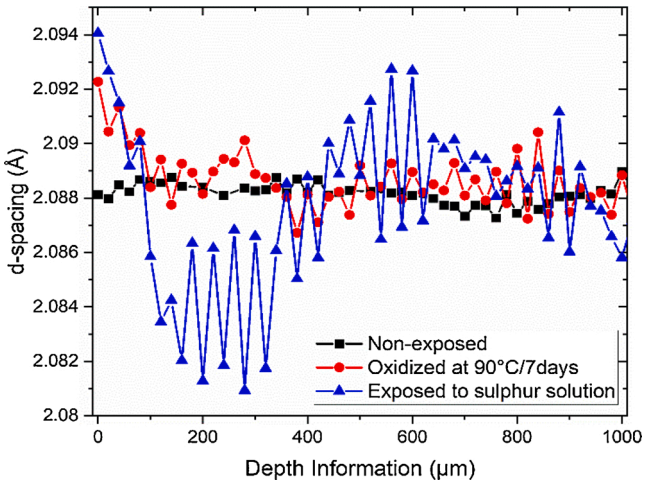

Fig. 5. The measured d-spacings (integrated over the entire (111)-oriented 2D-diffraction ring) plotted against the depth from the surface of the copper specimens.

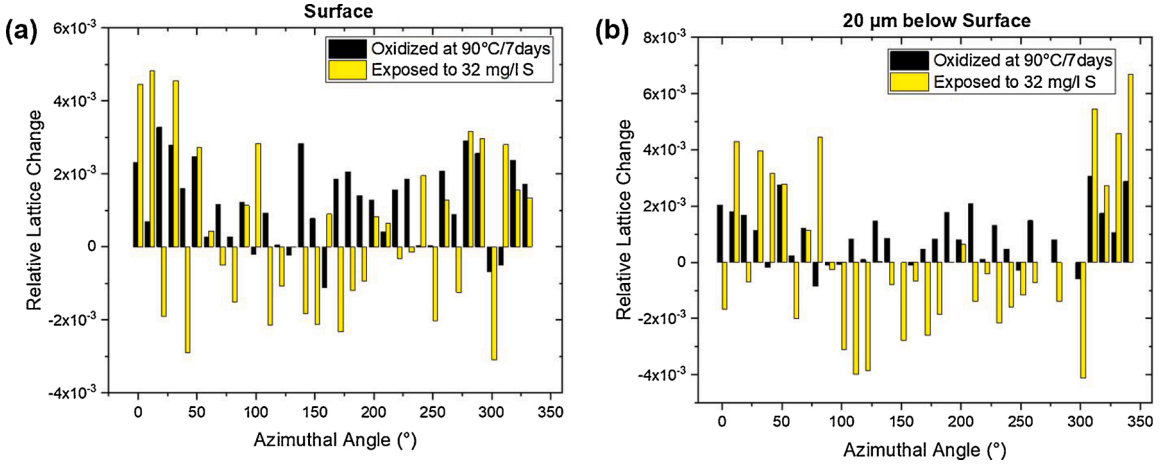

Fig. 4. The calculated relative change of lattice parameter in (a) the near-surface region, and (b) 20 µm below the surface, for the pre-oxidized and the sulfur-exposed sample, respectively.

the sub-surface region at 20 μm (Fig. 4b), varying with azimuthal angle. The non-uniform lattice deformation is due to the large scatter in grain size in the microstructure, as explained above. A histogram figure summarizes the measured d-spacings for all tested specimens can be found in the supplementary material (Fig. S1), which shows the lattice degradation as surface and near-surface lattice expansion and the formation of compensating lattice contraction in the sub-surface, which was more severe for the sulfur-exposed Cu sample than the pre-oxidized one.

4.2. Lattice deformation of the near-surface region

Fig. 5 shows the measured *d*-spacings plotted against the depth, i.e., in-depth gradient, for the samples. The *d*-spacings were calculated from full-ring-integrated data, indicating the lattice expansion in the near-surface region caused by the pre-oxidation and the sulfur-exposure, which is evident by comparison with the non-exposed sample showing nearly constant *d*-spacing across the depth. The pre-oxidation led to lattice expansion of the near-surface region down to ~90 μm. The exposure to the sulfide-containing groundwater resulted in an altered surface layer of ~400 μm. The magnitude of lattice expansion was more pronounced for the sulfur-exposed sample, clearly demonstrating a lattice degradation effect induced by the sulfide-containing groundwater. In addition to lattice expansion of the near-surface region down to ~90 μm, the sulfur-exposure also led to lattice contraction (depth of 100−400 μm in Fig. 5) beneath the lattice expansion near-surface region. However, the pre-oxidized sample did not show a similar compensation effect; therefore, the mechanism for the sub-surface lattice contraction must be of a different nature. The pronounced lattice contraction in the sulfur-exposed sample might have been generated due to compensation of lattice expansion of the near-surface region.

It is well-known that the pre-oxidation causes the formation of copper oxides, typically CuO/Cu_2O, on the Cu surface. The oxides have higher lattice constants and thus lead to a widening of the Cu lattice underneath the oxides. However, the thickness of the oxide film was reported to be only a few hundreds of nm [42,43]. Our HEXRD results, shown in Fig. 5, suggest that the pre-oxidation causes significant lattice deformation in the near-surface region down to 90 μm in depth. The surface grains became distorted, which led to the evolution of macro-strains. Note that the sulfur-exposed sample was also pre-oxidized; therefore, the measured data represent the effects of the pre-oxidation and sulfidation occurred during the exposure to the simulated groundwater. Therefore, the difference between these two samples shows the effect of interactions of the pre-oxidized sample with the sulfide-containing groundwater. The data of the sulfur-exposed sample show that the relative change of the lattice parameter in the surface region reaches a magnitude of 10^{-3}, indicating a high level of lattice deformation developed in the surface region, which can be explained by considering the H-induced lattice dilation.

The fitting results of the full-ring diffraction data in Fig. 6 revealed that the full-width at half maximum (FWHM) values of all Bragg peaks increased by the pre-oxidation and exposure to the S-containing water, with the latter having the most severe effect. Increase of FWHM typically indicates the formation of micro-deformation, i.e., the deformation within grains, and/or the reduction of the grain size. The deformation of the surface layer due to the formation of corrosion products result in heterogeneous grain deformation, which is reduced with increasing depth in bulk. However, the exposure to the S-containing water resulted in larger surface deformation (lattice expansion) and also sub-surface deformation (lattice contraction). The oxidation on the surface was rather homogeneous and caused a widening of the lattice, but the degradation caused by the exposure to the S-containing water exhibited a more heterogeneous nature. During the exposure to the simulated groundwater, Cu sulfides can form as a result of the corrosion of Cu. Moreover, pre-formed Cu_2O film can also be converted to the Cu_2S film, which was reported to extend into the bulk of Cu for about 100 nm from

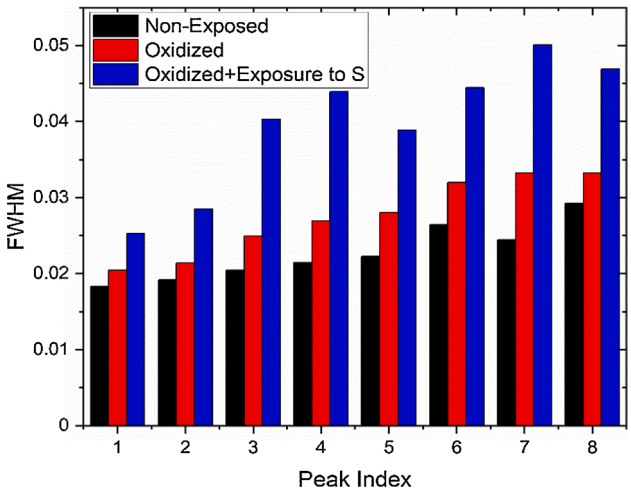

Fig. 6. Full-width at half maximum (FWHM) values from all measured diffraction peaks for the analyzed copper specimens, averaged over the entire sample thickness.

the surface [28]. However, the formation of corrosion products alone cannot explain the large lattice deformation, in particular, not the sub-surface lattice contraction observed in the sulfur-exposed sample. There are, apparently, other effects that resulted in the sub-surface lattice degradation. H and S can absorb and enter into Cu lattice, and their ingress is most favored at grain boundaries. Most likely, the H and S ingress caused the lattice degradation observed in the sulfur-exposed sample.

4.3. Adsorption of H_2S, HS, S, H on Cu(110) surface

In the assessment of corrosion risk of the Cu canister during long-term geological disposal, a key question is the corrosion of material integrity caused by S and H because of their presence in the groundwater in bedrock. DFT calculation of adsorption energies of H_2S, HS, S, H on Cu (110) surface was performed. Fig. 7 shows the calculated adsorption energies (binding strength) and corresponding models for the adsorbate species on Cu(110) surface. As seen in Fig. 7a, individual S atom adsorbs on the Cu(110) surface with adsorption energy (E_{ad}) of −1.5 eV, indicating a strong interaction between S and Cu surface. Compared to one S atom, H_2S molecule shows a low affinity towards Cu surface, the adsorption energy of which agrees well with the calculated value reported in the literature [44,45], while the adsorption energy of HS group is −0.7 eV, slightly lower than that of H_2S [45]. For a single H atom on Cu, a weak binding strength is found, with an adsorption energy of −0.2 eV, agreeing well with the literature [44]. By contrast, H_2S in its full dissociation form, i.e., H_S_H, significantly enhances the adsorption strength, and so is the dissociated HS (H_S), indicating a synergistic effect of H and S on the adsorption onto the Cu surface. Moreover, dissociation of H_2S into H_S_H and HS into H_S most likely proceeds spontaneously on the Cu surface, indicated by the large energy differences.

4.4. Insertion of H into Cu(110) lattice

Vacancies and interstitial atoms are two types of point defects in metals, which render the infusion of atoms from the environment into metal lattice. Interstitial H in metal is utilized for hydrogen storage, in which H dissolves in the metal lattice as solute and thus form hydride [46]. In general, atomic infusion can induce a large strain within metals, which may eventually lead to material rupture [47,48]. Here, we performed DFT calculation to investigate H insertion into Cu(110) lattice via the two types of defects, i.e., Cu vacancy or interstitial site,

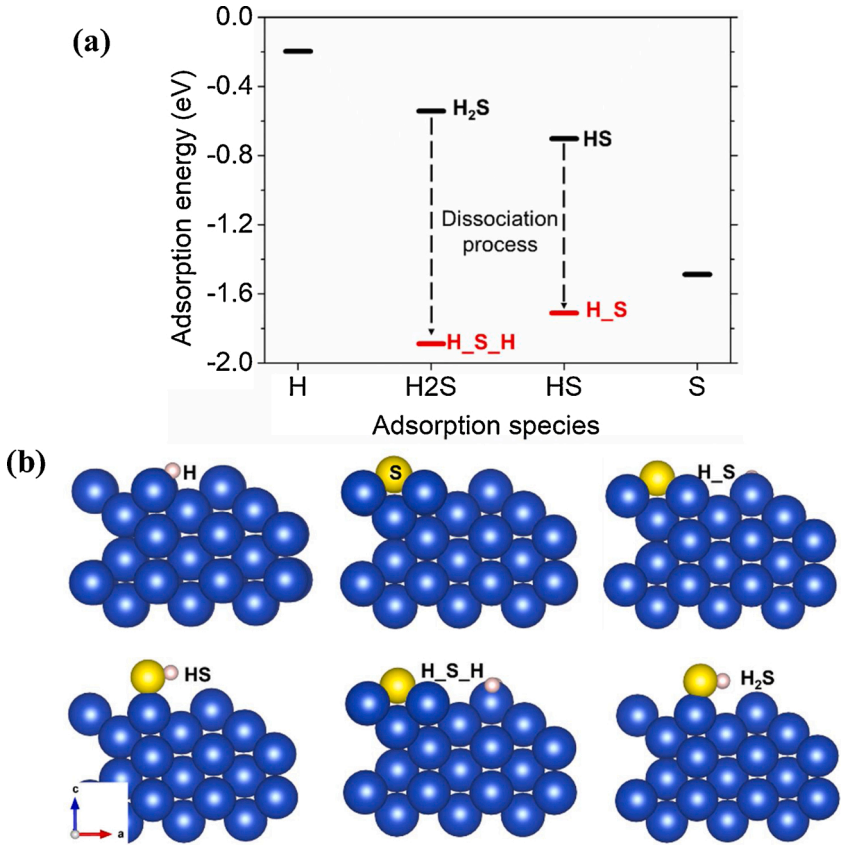

Fig. 7. (a) Calculated adsorption energies (E_{ad}) of H_2S and HS in their molecular form (H_2S, or HS), and full dissociation form (H_S_H, or H_S), and of individual S and individual H. (b) The adsorption configurations of molecular/dissociated H_2S/HS after optimization are depicted in side view, with yellow, light pink, and blue balls representing S, H, and Cu atoms.

respectively. First, individual H atom was introduced into Cu(110) via a Cu vacancy located at different depths, i.e., 1st, 2nd and 3rd atomic layer, denoted as the case "vac" in the modeling. Structure models with one H atom located at an interstitial site at 1st, 2nd and 3rd atomic layers are showing in Fig. 8a. While H stayed at nearly the same location in the first and third layer, the calculated insertion energies indicate that such insertion via vacancy is energetically unfavorable, as shown in Fig. 8b. In the case when H is inserted into a vacancy at the second atomic layer, after optimization the H atom moved up and stayed above the surface, suggesting a transition from "insertion" mode to "adsorption" mode, which resulted in a more stable configuration (binding energy of H on Cu surface is −0.36 eV) compared to the other two cases. This indicates that Cu vacancy promotes H adsorption, as compared to H adsorption on perfect Cu(110) surface (binding energy is −0.2 eV, see Fig. 8b). Furthermore, by introducing one vacancy next to the H atom, the insertion energy is slightly reduced and even to a native value (favorable) when the vacancy is at the same atomic layer as the H atom (Fig. 8b). The models as well as insertion energy corresponding to an

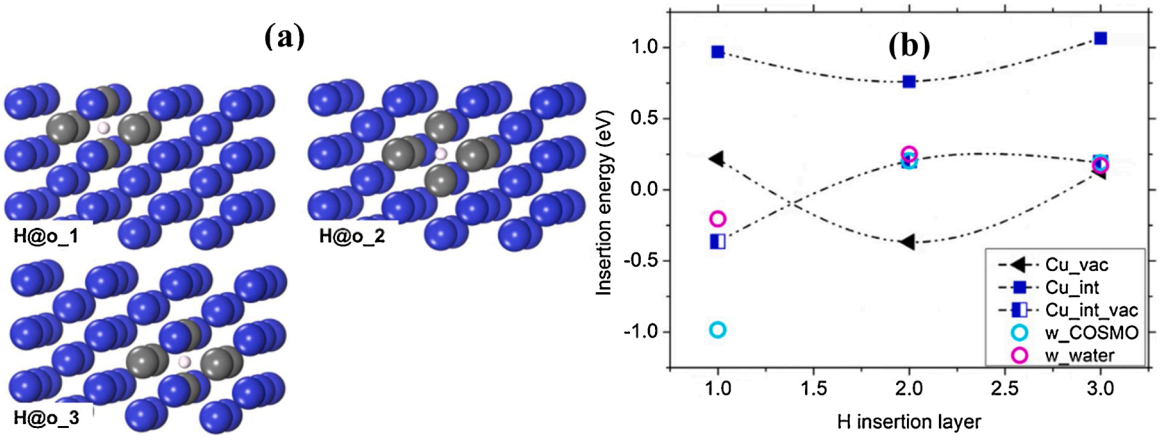

Fig. 8. (a) Models of Cu(110) surface with one H at 1st, 2nd and 3rd atomic layers denoted as H@o_1, H@o_2, H@o_3, respectively. The six Cu atoms comprising the octahedron around H atom (in light pink) are highlighted in grey, whereas other Cu atoms are in blue. (b) Insertion energy of H at a vacancy (case "vac"), an interstitial site (case "int"), and at an interstitial site accompanied by a vacancy (case "vac_int") in Cu(110) at 1st, 2nd and 3rd atomic layers. The effect of both implicit and explicit solvation is considered within the scheme of the "vac_int" case.

extra vacancy at different atomic layers can be found in the supplementary material (Fig. S2).

On the other hand, it is more likely that small atoms insert into metal lattice by occupying interstitial sites. For face-centered cubic metals like copper, its octahedral interstitial sites are usually more accessible for accommodation of small solute atoms. Here we only consider the octahedral interstitial site, the most favorable occupation site of H atom, as an example to show the energetical as well as structural characters of H insertion. The local structure comprised by the H atom and six surrounding Cu atoms are shown in Fig. 9a, and calculated lattice relaxation (expansion or contraction) along different directions are shown in Fig. 9b–d. For the interstitial H atom alone (case "int") without vacancy, the calculated insertion energy is higher (less favorable) compared to the vacancy case discussed above, see Fig. 8b. This could be attributed to large local relaxations within Cu lattice caused by H insertion. Further modeling was done by introducing an extra vacancy besides the H atom (case "vac_int"). Three situations with different relative locations between the H atom and the vacancy were considered, i.e., the vacancy is located at the upper layer, lower layer, or the same layer as the H atom. The results show that only when the vacancy is at the same layer as the H atom, it could significantly stabilize the H insertion (negative insertion energy, Fig. 8b). This can be understood by considering the almost vanished relaxations (especially in the z-direction) when a neighboring Cu vacancy is present, shown as "With vacancy" in Fig. 9b–d. A complete depiction of insertion energy data for different vacancy positions at different atomic layers can be found in the supplementary material (Fig. S3).

In the ideal case, the smallest and biggest distance between two Cu atoms within the local octahedron (Fig. 9a) are 2.578 Å and 3.646 Å, respectively. With one H atom staying at the center of this octahedron after optimization, positive relaxation in the z-direction (i.e., normal to Cu surface) is 17~22 % of the original atomic distance (Cu_0-Cu_5), significantly larger than that in x- or y-direction (Fig. 9b–d). Such large positive relaxations imply that the whole structure in z-direction must bear a large lattice dilation. On the other hand, H-induced relaxation in x-direction decreases as the H atom moves into inner layers, probably due to that the surface allows larger deformation. In contrast, relaxations in the y-direction are negligibly small (Fig. 9b–d). These calculations suggest that H insertion in octahedral interstitial sites generates strains in an anisotropic way, providing certain evidence for our experimental observations. Moreover, the enlarged Cu—Cu bond length and the lattice relaxation in x, y, and z1/z2 directions induced by H insertion, shown in Fig. 9, indicate a decrease of the metal bond strength, although the local relaxation/bond decrease may not be reflected in the averaged Cu bond strength.

Additionally, both implicit and explicit water environments were included in the modeling to investigate their influence on H insertion into Cu lattice. In the implicit water model, water molecules are treated as a continuum medium (COSMO) model [49,50], whereas in the explicit water model, two monolayers of water molecules (equal to twelve water molecules on the Cu slab) were considered in the calculation. For thick water layers, explicit water models become too difficult for the calculation, while the implicit water model is a good approximation of aqueous environments since water molecules are treated as a continuous aqueous layer. It turns out that the water solvation barely influences the insertion energy, except in the case when H lies at the first octahedral interstitial site under implicit water environment, where the insertion energy decreases largely to a negative value around −1 eV (Fig. 8b). In this case, the water environment causes a considerable reconstruction of the Cu surface, with a surface Cu atom occupying the subsurface Cu vacancy, as illustrated in Fig. 10, which is not observed in the non-solvation case. Such reconstruction could be responsible for the large decrease of the insertion energy. When the H atom moves deeper into the Cu lattice, the effect of solvation on the insertion energy quickly weakens (Fig. 8b).

4.5. *Diffusion of H in Cu*

The diffusion of H, S, and O in Cu, and self-diffusion of Cu have been reviewed concerning the safety assessment of the copper canister [51]. The transport mechanism and kinetics of these elements depend on the service condition, such as temperature and time [52]. Cu and S are substitutional elements and their diffusion takes place through the movement of point defects in the crystalline lattice. Lattice diffusion via

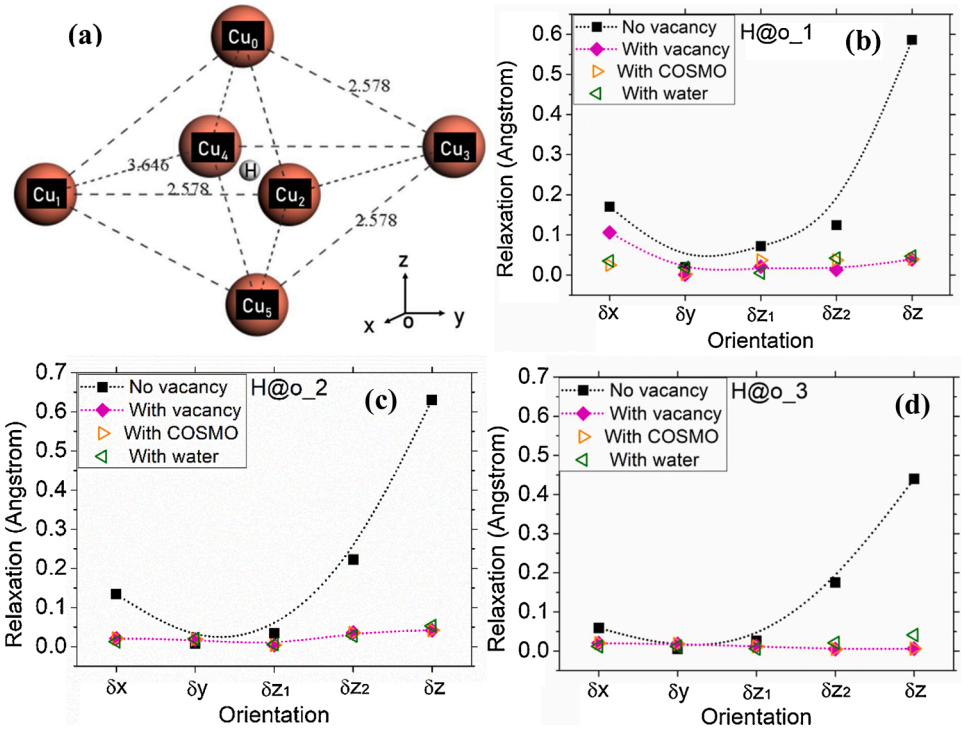

Fig. 9. (a) Configuration (before optimization) with one H atom located at the center of the octahedron comprised by six Cu atoms, which gives initial atomic distances between two Cu atoms: $Cu_{1\text{-}4} = Cu_{2\text{-}3} = 3.646$ Å (x direction), $Cu_{1\text{-}2} = Cu_{3\text{-}4} = 2.578$ Å (y direction), while Cu_0 and Cu_5 are both 2.578 Å away from the other four Cu atoms (denoted as z_2, z_1 direction, respectively); $Cu_{0\text{-}5} = 2.578$ Å is denoted as z direction. (b)~(d) Comparison between the relaxations induced by H insertion within o_1, o_2, o_3 under differed situations.

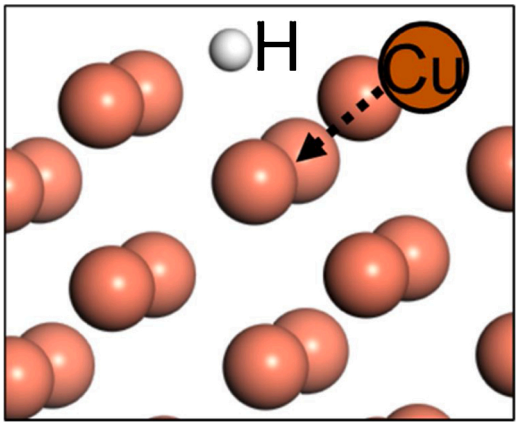

Fig. 10. A snapshot shows a surface Cu atom moves to and finally occupies a subsurface Cu vacancy when H atom is located at the first octahedral interstitial site.

vacancy is the dominating mechanism for diffusion of such large substitutional elements in metals at high temperatures. At temperatures below 100 °C, however, diffusion of Cu and S occurs almost entirely along grain boundaries, and the diffusivity of S is higher than the self-diffusion of Cu. S has very low solubility in Cu due to the formation of sulfides, which is a pinning effect. Estimated by using the diffusion data at room temperature, it takes 100,000 years for S and more than a million years for Cu to diffuse 5 cm distance (the thickness of the canister) along the grain boundaries in Cu [51].

O and H are the interstitial elements that can permeate the whole material via the interstitial sites. The interstitial diffusion occurs typically much faster than substitutional diffusion. However, similar to S, the solubility of O in Cu is very low at ambient temperature due to the formation of oxides. There are experimental data of self-diffusion of Cu at grain boundaries down to 250 °C [53], whereas no experimental data of S and O diffusion in Cu below 500 °C can be found because that is not detectable [51]. Thus, diffusion of S, O, and Cu is negligible at ambient temperature [51,52]. In contrast, H produced from the sulfide-induced corrosion of Cu can diffuse into the Cu [54], along the grain boundaries and also through the grains of Cu lattice. H has high mobility and permeability down to room temperature [55], and hydrogen depth profiles in hydrogen-charged copper specimens could be measured [35,36]. H diffusion in Cu lattice is much faster than S and O. By using the diffusion data in [51], it is estimated that H diffusion in Cu can reach 5 cm diffusion distance within 1000 years at room temperature. Based on the literature reports about H, S and O diffusion in Cu reviewed recently [56], only H diffusion in Cu lattice is considerable in our system.

4.6. H-induced lattice deformation and its implications

During long-term storage in the repository of the Cu canister, H may be produced on the Cu surface in contact with the groundwater by multiple processes. Microbiological activity in the vicinity, near-field and far-field [12,14,16,57], or on the surface of the canister if the bentonite barrier is damaged [15,19–21], produce sulfide species (mainly HS^- ions), and dissociation of the sulfide species on the Cu surface releases atomic S and H, which is a spontaneous process according to the DFT calculation [45, and this work]. Moreover, sulfide-induced corrosion reaction of Cu can generate H on the surface [24,25]. Furthermore, atomic H can also be produced at water/Cu interface through radiolysis of water, and it has been reported that gamma radiation from spent nuclear fuel greatly increases the H infusion into Cu, up to several orders of magnitudes depending on the dose of the radiation [10,11]. The DFT calculations suggest that H adsorption on Cu is energetically favorable, and co-existence with S promotes the H adsorption. H diffusion into Cu via interstitial sites is enhanced in the presence of vacancies in the Cu lattice. Moreover, water environment leads to a reconstruction of Cu surface, which facilitates the H insertion into Cu lattice. Thus, there is a risk for H-induced damage of the copper material associated with H infusion.

H absorption and diffusion in Cu are affected by the microstructure, and H can be trapped in defects such as grain boundaries and dislocations. H atoms entering the Cu material may lead to formation of voids and bubbles [30,34], and also enhance the creep rate and formation of microcracks showing an intergranular dimpled fracture [58,59]. At atomic level, H insertion into Cu lattice via interstitial sites leads to local lattice dilation, which also indicates a weakening of the Cu—Cu bond strength, implying a tendency for embrittlement. In the Cu material, the grains have different sizes and orientations, and the H-induced lattice deformation may vary and distribute heterogeneously in the microstructure. The lattice dilation due to H insertion is not directly related to macroscopic stress; however, if there is a depth gradient, then stresses may arise, which changes the lattice spacing. So changes of lattice spacings have two superimposed reasons: lattice dilation from H insertion and stresses caused by heterogeneous hydrogen distribution. Therefore, as a result of these two effects, H infusion can lead to the formation of a macroscopic lattice expansion, especially when accumulated in the surface region leading to a depth gradient.

The HEXRD measurements in this work show that deformation of Cu lattice induced by the 2-month exposure to the simulated groundwater occurred from the surface and extended deep into the bulk. The most lattice widening and lattice expansion occurred in the near-surface region down to 90 μm into the bulk. Based on the solubility and diffusion data, only H infusion could explain the measured Cu lattice deformation of this length scale, and the DFT calculation provides support for H-induced expansion of the Cu lattice. In this case, the hydrogen originated only from the corrosion reactions occurring during the exposure. The water environment facilitated the surface degradation, and S diffusion via grain boundaries may have contributed to the lattice deformation in the near-surface region. The measurement results provide clear evidence for highly heterogeneous lattice deformation, which is due to the microstructural heterogeneities in the Cu material. The tensile strain/stress curves were measured for the Cu material in sulfide-containing synthetic seawater, which show initial yielding starting at about 70 MPa and the maximum stress after about 40 % deformation is about 170 MPa [17]. Taking Young's modulus as 120 GPa, the respective elastic strains are 6×10^{-4} and 1.4×10^{-3}. These numbers should be considered as macroscopic averages over many grains. It was concluded that the Cu material is susceptible to intergranular attack (selective grain boundary dissolution) at low sulfide concentration (<0.005 M) and SCC at higher sulfide concentration (0.01 M). Recent experimental studies have confirmed the susceptibility of the Cu material to intergranular attack and SCC at high sulfide concentration [8,9]. In our work, without hydrogen charging and without applied strain, the two months exposure in the sulfide-containing groundwater already led to highly heterogeneous lattice deformation in the microstructure, and the measured lattice expansion in the surface region (within a depth of 90 μm) reached a magnitude of 10^{-3}, which shows the risk for a transition from elastic to plastic deformation and thus initiation of cracks at individual local sites.

Hydrogen-induced strain localization was observed in the Cu material in the initial stage of plastic deformation [60], and friction stir welding to seal the canister was found to increase hydrogen uptake in the weld zone and lead to strain localization near the weld zone [61]. Most likely, hydrogen infusion and associated local strain development play an important role in the reported susceptibility of Cu to SCC in the ground water containing sulfide [8,9,17]. During long-term storage in the repository of the Cu canister in the ground water containing sulfides, the sulfide-induced corrosion and hydrogen infusion may occur and lead to local strain development to a significant level and extend to a considerable depth. At grain boundaries in the surface region (interface between Cu and corrosion product), the H infusion and associated local tensile strain may lead to the initiation of microcracks, as reported in the

literature [30,34,58,59]. In a review report focusing on SCC of copper canisters, a conclusion of low risk for SCC was made based on considerations of classical SCC mechanisms caused by SCC agents (ammonia, acetate, nitrite, etc.), but the role of hydrogen in the sulfide-induced corrosion was ignored [62]. In the safety assessment reports, the corrosion allowance calculation mainly considers the rates of uniform corrosion in different forms [5,12,13]. For the sulfide-induced corrosion, the consequence was calculated as uniform corrosion thickness based on the amount of sulfur-species that reacts with copper and forms copper sulfide (Cu_2S) on the surface [54], without considering the effect of hydrogen that can enter the copper material. However, our HEXRD measurements clearly demonstrate the risk for H-induced SCC of the Cu material exposed to sulfide-containing groundwater. The DFT calculations provide a fundamental understanding of the role of S and H in the lattice degradation (embrittlement), which can result in highly heterogeneous microstructure degradation in the near-surface region leading to SCC of the canister. Considering the new findings from this work and recent studies of S- and H-induced corrosion and SCC [8,9,19–21,45,60,61], in the safety assessment of Cu canister, the risk for such complex forms of corrosion, i.e., SCC and hydrogen embrittlement, must be considered based on the state-of-the-art of the knowledge. Since the level of sulfide is a crucial issue, further studies are needed to improve our understanding at the atomic level in order to fully assess the risk for SCC and hydrogen embrittlement of Cu canister induced by sulfide-species in the groundwater, and by the radiation of spent fuel, alone and combined. It is necessary to consider not only the general corrosion as measured by the formation of corrosion products on the surface, but also the consequence of SCC and hydrogen embrittlement induced by H infusion into the Cu lattice and the influence of the microstructure.

5. Conclusion

Synchrotron HEXRD measurement and *ab initio* DFT calculation were combined to investigate the effects of pre-oxidation and exposure to simulated anoxic groundwater containing sulfide on the degradation of the lattice of the Cu material. The HEXRD measurement yielded 3-dimensional *d*-spacing data of the Cu samples, showing heterogeneous lattice deformation. The DFT calculation provided energetics of adsorption of H and S on Cu surface, as well as lattice relaxation induced by H insertion via interstitial sites in Cu lattice. The following conclusions can be drawn:

- The pre-oxidation of the Cu sample caused a lattice expansion mainly in the near-surface region ca. 90 μm deep.
- The exposure to the sulfide-containing simulated anoxic groundwater for two months caused a significant lattice deformation extending several hundreds of μm into the bulk, with an in-depth gradient of lattice expansion in the near-surface region ca. 90 μm deep and lattice contraction beneath the expansion region.
- Dissociation of H_2S and HS are exothermic processes, indicating spontaneous adsorption of H, H_S and H_S_H on Cu surface. The presence of S promotes the adsorption of H on the Cu surface.
- Water environment causes a considerable surface reconstruction of Cu lattice, leading to a large decrease in the insertion energy of H in the surface layer facilitating H ingress.
- H insertion via interstitial sites in Cu lattice occurs preferably in the presence of vacancies, and causes lattice expansion, mainly in the vertical direction to the surface. H insertion leads to a weakening of Cu-Cu bond strength.
- Only H infusion can explain the measured lattice dilation in the surface region after the exposure to the S-containing simulated anoxic groundwater, which indicates a risk for H-induced initiation of microcracks.
- As an overall implication the results clearly demonstrate the risk for H-induced SCC of Cu as canister material during long-term storage of nuclear fuel when exposed to sulfide-containing ground water.

Author statement

F.Z. performed the first literature survey, conducted the synchrotron experiments, and wrote the manuscript. C.Ö. conducted the synchrotron experiments, performed data analysis, and wrote the manuscript. M.L. performed DFT calculations, joined the synchrotron experiment, and wrote the manuscript. T.M. and U.L. supported and conducted the synchrotron experiments, and contributed to the manuscript writting. V. R.-H., L.C. and E.I. prepared the samples, performed corrosion exposure experiment, and contributed to the manuscript writing. J.P. acquired the funding, coordinated the project, planned and conducted experiments, and wrote the manuscript.

Data availability statement

The raw/processed data required to reproduce these findings will be shared by the corresponding author upon reasonable request.

Declaration of Competing Interest

The authors declare that they have no known competing financial interests or personal relationships that could have appeared to influence the work reported in this paper.

Acknowledgements

The financial support from NKS (Contract AFT/NKS-R(19)127/2) is greatly acknowledged. We are also grateful for the funding support from Swedish Research Council's program Röntgen-Ångström Cluster "In-situ High Energy X-ray Diffraction from Electrochemical Interfaces (HEXCHEM)" (project no. 2015-06092) and for PETRA III at DESY for providing the access to the beamline P21.2 for the HEXRD measurement. Moreover, we thank the Swedish National Infrastructure for Computing (SNIC) for providing the Swedish super-computing resource that enabled the DFT calculations.

Appendix A. Supplementary data

Supplementary material related to this article can be found, in the online version, at doi:https://doi.org/10.1016/j.corsci.2021.109390.

References

[1] Z.T. Wang Ju, Ten years progress of the radioactive waste disposal, The International Progress 7 (2003) 476.
[2] Design and Production of the KBS-3 Repository, SKB-TR-10-12, Swedish Nuclear Fuel and Waste Management Co., Sweden, 2010 updated in 2013.
[3] T. Saanio, A. Ikonen, P. Keto, T. Kirkkomäki, T. Kukkola, J. Nieminen, H. Raiko, Design of the Disposal Facility 2012, POSIVA-WR-13-17, Finland, 2013.
[4] T. Hedman, A. Nyström, C. Thegerström, Swedish containers for disposal of spent nuclear fuel and radioactive waste, C. R. Phys. 3 (2002) 903.
[5] F. King, C. Lilja, K. Pedersen, P. Pitkänen, M. Vähänen, An Update of the State-of-the-art Report on the Corrosion of Copper Under Expected Conditions in a Deep Geologic Repository, SKB-10-67, Swedish Nuclear Fuel and Waste Management Co., Sweden, 2010.
[6] C. Padovani, F. King, C. Lilja, D. Féron, S. Necib, D. Crusset, V. Deydier, N. Diomidis, R. Gaggiano, T. Ahn, P.G. Keech, D.D. Macdonald, H. Asano, N. Smart, D.S. Hall, H. Hänninen, D. Engelberg, J.J. Noël, D.W. Shoesmith, The corrosion behaviour of candidate container materials for the disposal of high-level waste and spent fuel – a summary of the state of the art and opportunities for synergies in future R&D, Corrosion Eng. Sci. Technol. 52 (2017) 227.
[7] A. Hedin, A.J. Johansson, C. Lilja, M. Boman, P. Berastegui, R. Berger, M. Ottosson, Corrosion of copper in pure O_2-free water? Corros. Sci. 137 (2018) 1.
[8] R. Becker, J. Öijerholm, Slow Strain Rate Testing of Copper in Sulfide Rich Chloride Containing Deoxygenated Water at 90 °C, SSM 2017:02, Swedish Radiation Authority, Sweden, 2017.
[9] R. Becker, A. Forsström, Y. Yagodzinskyy, H. Hänninen, M. Heikkilä, Sulphide-induced Stress Corrosion Cracking and Hydrogen Absorption in Copper Exposed to

Sulphide and Chloride Containing Deoxygenated Water at 90°C, SSM 2020:01, Swedish Radiation Authority, Sweden, 2020.
[10] C.M. Lousada, I.L. Soroka, Y. Yagodzinskyy, N.V. Tarakina, O. Todoshchenko, H. Hänninen, P.A. Korzhavyi, M. Jonsson, Gamma radiation induces hydrogen absorption by copper in water, Sci. Rep. 6 (2016) 24234.
[11] I. Soroka, N. Chae, M. Jonsson, On the mechanism of γ-radiation-induced corrosion of copper in water, Corros. Sci. 182 (2021), 109279.
[12] D.S. Hall, M. Behazin, W.J. Binns, P.G. Keech, An evaluation of corrosion processes affecting copper-coated nuclear waste containers in a deep geological repository, Prog. Mater. Sci. 118 (2021) 100766, https://doi.org/10.1016/j.pmatsci.2020.100766.
[13] Supplementary Information on Canister Integrity Issues, SKB TR-19-15, Swedish Nuclear Fuel and Waste Management Co., Sweden, 2019.
[14] F. King, M. Kolar, I. Puigdomenech, P. Pitkänen, C. Lilia, Modeling microbial sulfate reduction and the consequences for corrosion of copper canisters, Mater. Corros. 72 (2021) 339.
[15] L. Carpén, P. Rajala, E. Huttunen-Saarivirta, M. Bomberg, Corrosion behavior of copper in simulated anoxic groundwater inoculated with sulfate reducing bacteria and methanogens. Corrosion 2017, NACE International, New Orleans, Louisiana, USA, 2017, p. 15.
[16] K. Pedersen, Microbial Processes in Radioactive Waste Disposal, SKB-TR-00-04, Swedish Nuclear Fuel and Waste Management Co., Sweden, 2000.
[17] N. Taniguchi, M. Kawasaki, Influence of sulfide concentration on the corrosion behavior of pure copper in synthetic seawater, J. Nucl. Mater. 379 (2008) 154.
[18] E. Huttunen-Saarivirta, P. Rajala, L. Carpén, Corrosion behaviour of copper under biotic and abiotic conditions in anoxic ground water: electrochemical study, Electrochim. Acta 203 (2016) 350.
[19] L. Carpén, P. Rajala, M. Bomberg, Corrosion of copper in anoxic ground water in the presence of SRB, Corros. Sci. Technol. 17 (2018) 147.
[20] E. Huttunen-Saarivirta, E. Ghanbari, F. Mao, P. Rajala, L. Carpén, D.D. Macdonald, Kinetic properties of the passive film on copper in the presence of sulfate-reducing bacteria, J. Electrochem. Soc. 165 (2018) C450.
[21] E. Huttunen-Saarivirta, P. Rajala, M. Bomberg, L. Carpén, Corrosion of copper in oxygen-deficient groundwater with and without deep bedrock micro-organisms: characterization of microbial communities and surface processes, Appl. Surf. Sci. 396 (2017) 1044.
[22] D. Kong, C. Dong, A. Xu, C. Man, C. He, X. Li, Effect of sulfide concentration on copper corrosion in anoxic chloride-containing solutions, J. Mater. Eng. Perform. 26 (2017) 1741.
[23] J. Chen, Z. Qin, D. Shoesmith, Long-term corrosion of copper in a dilute anaerobic sulfide solution, Electrochim. Acta 56 (2011) 7854.
[24] T. Martino, R. Partovi-Nia, J. Chen, Z. Qin, D.W. Shoesmith, Mechanisms of film growth on copper in aqueous solutions containing sulphide and chloride under voltammetric conditions, Electrochim. Acta 127 (2014) 439.
[25] J. Chen, Z. Qin, D. Shoesmith, Kinetics of corrosion film growth on copper in neutral chloride solutions containing small concentrations of sulfide, J. Electrochem. Soc. 157 (2010) C338.
[26] J. Chen, Z. Qin, T. Martino, M. Guo, D. Shoesmith, Copper transport and sulphide sequestration during copper corrosion in anaerobic aqueous sulphide solutions, Corros. Sci. 131 (2018) 245.
[27] J. Smith, J. Wren, M. Odziemkowski, D. Shoesmith, The electrochemical response of preoxidized copper in aqueous sulfide solutions, J. Electrochem. Soc. 154 (2007) C431.
[28] H. Hollmark, P. Keech, J. Vegelius, L. Werme, L.-C. Duda, X-ray absorption spectroscopy of electrochemically oxidized Cu exposed to Na_2S, Corros. Sci. 54 (2012) 85.
[29] J. Condon, T. Schober, Hydrogen bubbles in metals, J. Nucl. Mater. 207 (1993) 1.
[30] T. Nieh, W. Nix, The formation of water vapor bubbles in copper and their effect on intergranular creep fracture, Acta Metall. 28 (1980) 557.
[31] S. Nakahara, Microscopic mechanism of the hydrogen effect on the ductility of electroless copper, Acta Metall. 36 (1988) 1669.
[32] Y. Okinaka, H. Straschil, The effect of inclusions on the ductility of electroless copper deposits, J. Electrochem. Soc. 133 (1986) 2608.
[33] J. Angeli, A. Bengtson, A. Bogaerts, V. Hoffmann, V.-D. Hodoroaba, E. Steers, Glow discharge optical emission spectrometry: moving towards reliable thin film analysis–a short review, J. Anal. At. Spectrom. 18 (2003) 670.
[34] M. Ganchenkova, Y. Yagodzinskyy, V. Borodin, H. Hänninen, Effects of hydrogen and impurities on void nucleation in copper: simulation point of view, Philos. Mag. 94 (2014) 3522.
[35] Å. Martinsson, R. Sandström, C. Lilja, Hydrogen in Oxygen-free, Phosphorus-doped Copper: Charging Techniques, Hydrogen Contents and Modelling of Hydrogen Diffusion and Depth Profile, SKB-TR-13-09, Swedish Nuclear Fuel and Waste Management Co., Sweden, 2013.
[36] Å. Martinsson, R. Sandström, Hydrogen depth profile in phosphorus-doped, oxygen-free copper after cathodic charging, J. Mater. Sci. 47 (2012) 6768.
[37] E. Isotahdon, L. Carpen, P. Rajala, Corrosion of copper in geological repository for nuclear waste - the effect of oxic phase on the corrosion behaviour of copper in anoxic environment, in: The European Corrosion Congress, EUROCORR 2019, 2019.
[38] G. Ashiotis, A. Deschildre, Z. Nawaz, J.P. Wright, D. Karkoulis, F.E. Picca, J. Kieffer, The fast azimuthal integration Python library: pyFAI, J. Appl. Crystallogr. 48 (2015) 510.
[39] B. Delley, An all-electron numerical method for solving the local density functional for polyatomic molecules, J. Chem. Phys. 92 (1990) 508.
[40] B. Delley, From molecules to solids with the DMol 3 approach, J. Chem. Phys. 113 (2000) 7756.
[41] J.P. Perdew, J.A. Chevary, S.H. Vosko, K.A. Jackson, M.R. Pederson, D.J. Singh, C. Fiolhais, Atoms, molecules, solids, and surfaces: applications of the generalized gradient approximation for exchange and correlation, Phys. Rev. B 46 (1992) 6671.
[42] M. O'reilly, X. Jiang, J. Beechinor, S. Lynch, C. NíDheasuna, J. Patterson, G. Crean, Investigation of the oxidation behaviour of thin film and bulk copper, Appl. Surf. Sci. 91 (1995) 152.
[43] C. Gattinoni, A. Michaelides, Atomistic details of oxide surfaces and surface oxidation: the example of copper and its oxides, Surf. Sci. Rep. 70 (2015) 424.
[44] Q.L. Tang, H_2S splitting on Cu (110): insight from combined periodic density functional theory calculations and microkinetic simulation, Int. J. Quantum Chem. 113 (2013) 1992.
[45] C.M. Lousada, A.J. Johansson, P.A. Korzhavyi, Molecular and dissociative adsorption of water and hydrogen sulfide at perfect and defective Cu (110) surfaces, Phys. Chem. Chem. Phys. 19 (2017) 8111.
[46] U. Eberle, M. Felderhoff, F. Schueth, Chemical and physical solutions for hydrogen storage, Angew. Chemie Int. Ed. 48 (2009) 6608.
[47] F. Fujita, T. Sohmura, Hydrogen in stainless steel and Fe-Ni alloys, Le Journal de Physique Colloques 37 (1976). C6-379-C6-383.
[48] R.H. Rusli, T. Fujita, Approximation of hydrogen induced delayed fracture of overlaid cladding in pressure vessels steel structure, J. Eng. Technol. Sci. 40 (2008) 110.
[49] A. Klamt, G. Schüürmann, COSMO: a new approach to dielectric screening in solvents with explicit expressions for the screening energy and its gradient, J. Chem. Soc. Perkin Trans. 2 (1993) 799.
[50] B. Delley, The conductor-like screening model for polymers and surfaces, Mol. Simul. 32 (2006) 117.
[51] H. Magnusson, K. Frisk, Self-diffusion and Impurity Diffusion of Hydrogen, Oxygen, Sulphur and Phosphorus in Copper, SKB TR-13-24, Swedish Nuclear Fuel and Waste Management, Sweden, 2013.
[52] H. Magnusson, K. Frisk, Thermodynamic Evaluation of Cu-H-O-S-P System - Phase Stabilities and Solubilities for OFP-copper, SKB TR-13-11, Swedish Nuclear Fuel and Waste Management Co., Sweden, 2013.
[53] D. Gupta, Comparative Cu diffusion studies in advanced metallizations of Cu and Al-Cu based thin films, MRS Online Proc. Lib. Arch. 337 (1994).
[54] Corrosion Calculations Report for the Safety Assessment SR-Site, SKB TR-10-66, Swedish Nuclear Fuel and Waste Management Company, Sweden, 2010.
[55] G. Caskey Jr, A. Dexter, M. Holzworth, M. Louthan Jr, R. Derrick, The effect of oxygen on hydrogen transport in copper, Corrosion 32 (1976) 370.
[56] H. Magnusson, K. Frisk, Diffusion, permeation and solubility of hydrogen in copper, J. Phase Equilibria Diffus. 38 (2017) 65.
[57] SR-Site – Sulphide Content in the Groundwater at Forsmark, SKB TR-10-39, Swedish Nuclear Fuel and Waste Management Co., Sweden, 2010.
[58] R. Wu, F. Seitisleam, R. Sandström, L. Jin, Creep Crack Growth in Phosphorus Alloyed Oxygen Free Copper, SKB R-11-11, Swedish Nuclear Fuel and Waste Management Co., Sweden, 2011.
[59] Y. Yagodzinskyy, E. Malitckii, T. Saukkonen, H. Hänninen, Hydrogen-enhanced creep and cracking of oxygen-free phosphorus-doped copper, Scr. Mater. 67 (2012) 931.
[60] Y. Yagodzinskyy, E. Malitckii, F. Tuomisto, H. Hänninen, Hydrogen-induced strain localization in oxygen-free copper in the initial stage of plastic deformation, Philos. Mag. 98 (2017) 727.
[61] A. Forsström, S. Bossuyt, Y. Yagodsinskyy, K. Tsuzaki, H. Hänninen, Strain localization in copper canister FSW welds for spent nuclear fuel disposal, J. Nucl. Mater. 523 (2019) 347.
[62] F. King, R. Newman, Stress Corrosion Cracking of Copper Canisters, SKB TR-10-04, Swedish Nuclear Fuel and Waste Management Co., Sweden, 2010.